Neuroinform (2007) 5:207–222
DOI 10.1007/s12021-007-9000-z

Inverse Current-Source Density Method in 3D: Reconstruction Fidelity, Boundary Effects, and Influence of Distant Sources

Szymon Łęski · Daniel K. Wójcik · Joanna Tereszczuk · Daniel A. Świejkowski · Ewa Kublik · Andrzej Wróbel

Published online: 27 November 2007

Abstract Estimation of the continuous current-source density in bulk tissue from a finite set of electrode measurements is a daunting task. Here we present a methodology which allows such a reconstruction by generalizing the one-dimensional inverse CSD method. The idea is to assume a particular plausible form of CSD within a class described by a number of parameters which can be estimated from available data, for example a set of cubic splines in 3D spanned on a fixed grid of the same size as the set of measurements. To avoid specificity of particular choice of reconstruction grid we add random jitter to the points positions and show that it leads to a correct reconstruction. We propose different ways of improving the quality of reconstruction which take into account the sources located outside the recording region through appropriate boundary treatment. The efficiency of the traditional CSD and variants of inverse CSD methods is compared using several fidelity measures on different test data to investigate when one of the methods is superior to the others. The methods are illustrated with reconstructions of CSD from potentials evoked by stimulation of a bunch of whiskers recorded in a slab of the rat forebrain on a grid of $4 \times 5 \times 7$ positions.

Keywords Current source density · Local field potentials · Evoked potentials · Inverse problems · Rat · Thalamus · Somatosensory system

S. Łęski (✉)
Center for Theoretical Physics, Polish Academy of Sciences,
al. Lotników 32/46, 02-668 Warsaw, Poland
e-mail: s.leski@nencki.gov.pl

S. Łęski · D. K. Wójcik · D. A. Świejkowski · E. Kublik · A. Wróbel
Department of Neurophysiology, Nencki Institute of Experimental Biology, Polish Academy of Sciences,
ul. Pasteura 3, 02-093 Warsaw, Poland

D. K. Wójcik
e-mail: d.wojcik@nencki.gov.pl

D. K. Wójcik · A. Wróbel
Warsaw School of Social Psychology,
ul. Chodakowska 19/31, 03-815 Warsaw, Poland

J. Tereszczuk
Faculty of Mathematics and Information Science,
Warsaw University of Technology,
Pl. Politechniki 1, 00-661 Warsaw, Poland

Introduction

One of the standard methods of analyzing extracellularly recorded local field potentials (LFPs) in neural tissue is the estimation of the current-source density (CSD) which generated them (Freeman and Nicholson 1975; Nicholson and Freeman 1975). The connection between the electric potential ϕ and the current-sources of density C is, under assumption of quasi-static regime (Mitzdorf 1985), given by the equation:

$$\nabla(\sigma \nabla \phi) = -C \,, \tag{1}$$

where σ is the electrical conductivity tensor (Plonsey 1969). In general, σ not only depends on position but is also anisotropic (Ueno and Sekino 2005). Since we do not know the properties of σ in the studied tissue in this work we assume that it is a constant scalar. This means

that the electrical conductance of the tissue is assumed homogeneous and isotropic.

The CSD is usually calculated in one dimension, for example if a laminar multielectrode is used to record evoked potentials in the cerebral cortex. In this case Eq. 1 reduces to

$$\sigma \frac{\partial^2 \phi}{\partial z^2} = -C(z) \, . \tag{2}$$

Let us assume that ϕ is measured at n equidistant electrode points with interelectrode distance h. The traditional method of estimating $C(z)$ at the *interior* points $z_i, i = 2, \ldots, n-1$ is to use the numerical second derivative (Mitzdorf 1985). This leads to

$$C(z_i) = -\sigma \frac{\phi(z_i + h) - 2\phi(z_i) + \phi(z_i - h)}{h^2} \, . \tag{3}$$

To calculate the CSD at the extreme points one may follow the suggestion of Vaknin et al. (1988) which is to assume that the potentials do not vary for $z < z_1$ and $z > z_n$, that is $\phi(z) = \phi(z_1)$ for $z < z_1$ and $\phi(z) = \phi(z_n)$ for $z > z_n$.

Recently, Pettersen et al. (2006) proposed a general framework called *inverse CSD method* (iCSD) which explicitly takes into account the assumptions made about the form of the sources. They observed that given the distribution of currents in the tissue it is formally a simple matter to evaluate the potentials measured at any point in space. One has to add up the contributions from every point source $I(x_0, y_0, z_0, t)$ which are of the form

$$\phi(x, y, z, t) = \frac{I(x_0, y_0, z_0, t)}{4\pi\sigma\sqrt{(x - x_0)^2 + (y - y_0)^2 + (z - z_0)^2}}.$$

Taking current-source distribution parameterized with parameters $\mathbf{C} = [C_1, \ldots, C_M]$ one gets a functional relation

$$\Phi = [\phi(\mathbf{x}_1) \ldots \phi(\mathbf{x}_N)] = F(\mathbf{C})$$

which can usually be inverted if the number of parameters, M, is equal to the number of measurement points, $\mathbf{x}_i \equiv (x_i, y_i, z_i)$, $i = 1..N$. Inverting this relation leads to the values of parameters $\mathbf{C}$ for a given set of measured potentials Φ. This is particularly convenient for parameterizations leading to F linear in C.[1]

The Inverse Current Source Density method is a generalization of the traditional Current Source Density method described above. Assume the potentials measured at equidistant points z_i through the cortex, $z_{i+1} - z_i = h$. Consider current sources distributed uniformly on infinitely extended and infinitely thin parallel planes passing through the measurement points and perpendicular to the electrode. Let C_i be the value of planar current source density at z_i divided by h, which would be the value of volume current-source density at this point if the current was distributed in the slice of thickness h instead. Then the potentials $\phi(z_i)$ are connected with the current-source parameters C_i by Eq. 3, see Pettersen et al. (2006).

Once the framework connecting C with ϕ is established it is natural to consider other distributions of current in the brain which would be more plausible than infinitely thin, infinitely extended planes of constant current-source density. Pettersen et al. considered three different choices of distributions leading to three variants of iCSD which they called "δ-source iCSD", "step iCSD", and "spline iCSD" methods. In the first case they assumed current sources distributed in infinitely thin discs of radius R passing through z_i. "Step iCSD" assumes current distribution in cylinders of radius R and height h centered at measurement points. The last method assumes a continuously varying in z but constant in the x, y plane profile of current-source density. In all these cases the CSD distribution is parameterized by its values at the measurement points. Let us stress that all these methods were developed for a one-dimensional problem of a multielectrode passing through the cortex perpendicularly to its surface.

Recently we performed experiments in which LFPs were measured at a three-dimensional array of $4 \times 5 \times 7$ points in order to reveal the dynamics and specificity of rat diencephalic activation which follows vibrissal stimulation. The simplest approach for examining three-dimensional CSD would be to generalize

[1] Note that the CSD in the whole tissue needs not be specified by its values on the grid, but, for instance, could be specified by the total current, position of the center and the spread of each of the sources. Then the potentials on the grid would be a nonlinear function of the parameters of CSD. Such a functional relation, however, would be of smaller practical utility in the application considered, which is why we restrict ourselves to the linear case. We believe it is useful to stress that the parameterizations can be more general as there may be other techniques, e.g. based on statistical learning, where nonlinear parametrization can be more natural and inverse of F is not required.

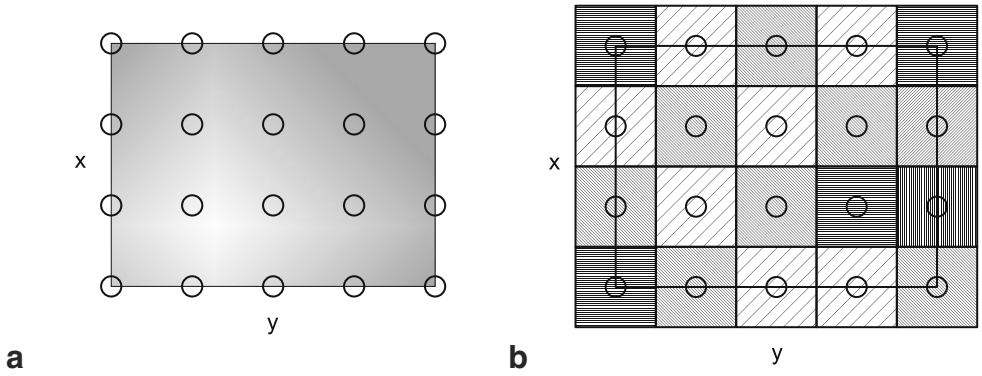

Fig. 1 The assumed distribution of current-sources (two-dimensional analog). *Circles* denote the grid points. We usually assume that the electrodes are located at, or very close to, the knots of the grid spanning CSD. **a** CSD at any point is an interpolation (linear or spline) of the values at the nodes. **b** In step method we assume constant CSD in a box around each node

the numerical second derivative and use an approximation to Laplacian:

$$C(x_i, y_i, z_i) = -\frac{\sigma}{h^2}\Big[\phi(x_i + h, y_i, z_i) + \phi(x_i - h, y_i, z_i) + \phi(x_i, y_i + h, z_i) + \phi(x_i, y_i - h, z_i) + \phi(x_i, y_i, z_i + h) + \phi(x_i, y_i, z_i - h) - 6\phi(z_i)\Big]. \quad (4)$$

This formula (in two dimensions) was used for example by Novak and Wheeler (1989), Shimono et al. (2000) and Lin et al. (2002). However, the traditional approach implies the exclusion of all the boundary points. In a typical one-dimensional recording the loss of two points out of 15–20 may be acceptable. In our case the boundary consists of 110 out of 140 measurement points. The procedure suggested by Vaknin (to assume the potentials do not change outside the grid) seemed not well justified in our experiments therefore we decided to generalize the inverse CSD method to three-dimensional case. An early attempt to get information about the three-dimensional distribution of the field in the cortex by Sukov and Barth (1998) combined analysis of measurements on 8×8 epipial electrode grid with laminar multielectrode depth recordings. The 16-point multielectrode was placed in the point which exhibited highest surfacial activity. Second order approximation to Laplacian with the Vaknin condition was used to obtain CSD at the measurement points. Other points in the bulk tissue were not probed hence the obtained CSD had a product structure and could not resolve the 3D structure of sources and sinks in the studied tissue.

All the figures and all the numerical examples in the subsequent sections use the grid $4 \times 5 \times 7$ which was also used in the experiment. The validity of the methods, however, is independent of the size of the grid.

Methods

The Inverse CSD Method in Three Dimensions

Let us start with a three-dimensional cubic grid of n_x, n_y and n_z points in respective directions so that each recording site (x_j, y_j, z_j) is close to one of the grid points.[2] We assume that the total number of electrodes is the same as the number of grid points and is equal to $n = n_x n_y n_z$. We then consider some class of current-source distributions with n free parameters. Such distributions can be parameterized by the n values of CSD at the grid points. One example is a piecewise constant (step) distribution: current-source density is constant in cubes of unit edge length centered on the grid points. Next we calculate the potentials at the electrodes locations generated by the assumed CSD distribution. This leads to a linear formula for each ϕ in terms of the n parameters of C of the form $\Phi = F\mathbf{C}$, where $\mathbf{C}$ stands for all the parameters organized in a vector. We finally invert this relation to calculate the n unknown parameters $\mathbf{C}$ (hence the whole CSD distribution) from the measured potentials. The exact form of this linear operator depends on the assumed form of the current sources distribution.

We consider a number of different CSD distributions. One is the step distribution described above. Another is based on linear approximation: we assume

[2] It is convenient to work with unit spacing and to include the true edge length h at the very end of the calculations, this is done simply by dividing the resulting CSD by h^2.

that the CSD is piecewise linear, that is the CSD between the grid points is calculated from the values at the nearest nodes via linear interpolation. The third case we study is the CSD distribution in the form of three-dimensional cubic splines with knots at grid points (that means the CSD in the whole volume is calculated from the values at grid points using spline interpolation). We consider two types of splines, "natural" and "not-a-knot", differing with a normalization condition (see the "Appendices"). We also considered variants of above distributions to deal with boundary effects. They are described in the following sections.

In the case of linear and spline distributions we assumed that the current-sources are localized inside the grid. In case of the step distribution the CSD is nonzero in a slightly larger cuboid spanned by all the unit-size boxes centered at grid points (see Fig. 1).

The calculation of the linear operator F for step distribution is quite simple. Let us denote the position of the i-th electrode by $(\tilde{x}_i, \tilde{y}_i, \tilde{z}_i)$ and the coordinates of the j-th grid node by (x_j, y_j, z_j). In general they need not be the same. Then the potential at i-th electrode location is given by

$$\Phi_i = \Phi(\tilde{x}_i, \tilde{y}_i, \tilde{z}_i) = \sum_{j=1}^{n} F_{ij} C_j,$$

where

$$C_j = C(x_j, y_j, z_j) \ .$$

The matrix element F_{ij} is the contribution of the uniform CSD of unit density located at a box centered at point j to the potential at point i. Thus, for the step distribution of CSD, it is given by

$$F_{ij} = \frac{1}{4\pi\sigma} \int_{x_j-1/2}^{x_j+1/2} \int_{y_j-1/2}^{y_j+1/2} \int_{z_j-1/2}^{z_j+1/2} \frac{\mathrm{d}z\mathrm{d}y\mathrm{d}x}{\sqrt{(\tilde{x}_i - x)^2 + (\tilde{y}_i - y)^2 + (\tilde{z}_i - z)^2}} \ . \tag{5}$$

This integral is easy to evaluate numerically, although one must be careful because of the singularity of the integrand.[3] Once we have the matrix F we can use its inverse to estimate the CSD at grid points from known potentials:

$$C_j = \sum_{i=1}^{n} (F^{-1})_{ji} \Phi_i \ .$$

These values define the whole CSD distribution.

The operator F for linear and spline methods is calculated similarly, although the calculations get much more complicated, especially for the cubic splines. For details of the calculations we refer the reader to "Appendices".

Boundary Effects and Distant Sources

In the linear and spline distributions described in the previous section it is assumed that CSD is non-zero only inside the cuboid enclosing the grid, which was chosen to approximate the distribution of electrode locations. In real tissue this assumption is not fulfilled: the array of electrodes covers only a small area of the brain and there are many sources outside that area. If we used the Laplacian to calculate CSD, then the influence of the outlying sources could be neglected. For example, if there was an additional distant point source then there would be a $\frac{1}{r}$ term in observed potentials, but $\nabla^2 \frac{1}{r} = 0$ which gives no contribution to the calculated CSD.[4] The situation is different with the inverse method. Here we have one-to-one correspondence (via operators F and F^{-1}) between sources and potentials, hence any additional term in the potentials (like $\frac{1}{r}$) will produce spurious sources. Nevertheless, it is possible to modify the inverse method in such a way that we can profit from its advantages over traditional CSD and at the same time limit the impact of the above mentioned effect.

To accommodate the sources located outside the electrode grid we extend the grid by one point in each direction, therefore an additional layer of non-zero CSD is created. The CSD at additional grid points is either zero, which we denote with the letter "B", or a duplication[5] of the boundary layer of the original grid, which is denoted by "D" (see Fig. 2). Therefore we have "linear", "linear B" and "linear D" methods, similarly

[3] We dealt with the singularity by simply excising a ball of radius $\varepsilon = 10^{-8}$ or $\varepsilon = 10^{-6}$. The numerical error introduced by such an excision is smaller than ε^2.

[4] Except at $r = 0$, which is not the case here because the source is "distant".

[5] Note that the larger grid has extra corner points which do not directly correspond to points in the original grid. For these corner points duplication means that we take the value at the closest (corner) point in the original grid. In other words, values at the corner points in the original grid are used at more than one point in the extended grid. A similar observation applies to the points on the edges of the grid.

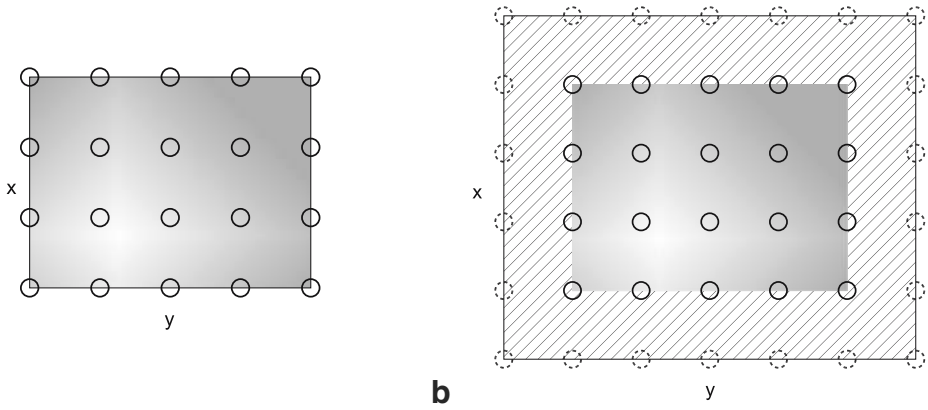

Fig. 2 Comparison of "standard" vs. B or D distribution of sources. In standard distribution **a** the CSD is non-zero only inside the grid of the same size as the number of electrodes, while in B or D distribution **b** there is an additional layer of non-zero CSD

for splines. In the context of laminar multielectrodes the "spline B" method was proposed by Pettersen et al. (2006). At the practical level the difference between these methods is that we use different matrices F. The modified linear operator F is constructed in three steps. First we act on a vector of n CSD values with a matrix B, which produces a larger vector (of size $N = (n_x+2)(n_y+2)(n_z+2)$) of CSD values on a larger grid. There are two different B matrices, B^B and B^D, for B and D boundary conditions respectively. Then we apply the matrix F calculated for the larger $(n_x+2)\times(n_y+2)\times(n_z+2)$ grid. In the final step we discard the values of potential at the boundary to get a vector of size n; this is done by applying a matrix R. Summarizing, we have the following formula for the F^B matrix (superscripts indicate the size of the grid for which the F matrix is calculated):

$$F^{n_x,n_y,n_z\ B} = RF^{(n_x+2),(n_y+2),(n_z+2)}B^B\ ,$$

analogously for F^D. Note that there is no point in considering "step B" method because it is the same as "step", however, we may consider "step D".

The B and D boundary conditions are motivated by the following heuristics. We know that the sources we deal with in real-world situations are not restricted to lie within the space spanned by the grid. Suppose therefore that there is a source outside, for example near a corner of the cuboid. This source will affect the potentials, especially in the corner. The inverse CSD method will then generate a current-source distribution *inside* the grid such that the resulting potential will match the one measured at the recording points. In other words, the method will try to imitate the outlying source with sources located inside the grid. This will lead to errors in CSD reconstruction, for example a false source in the corner may appear. Consider now the same potentials processed with a method using B boundary condition. One expects that the B method may also generate a spurious source in the corner, but the magnitude of the source will be smaller. This is because a larger CSD value in the corner means also larger CSD in the additional layer and the iCSD B method may place a smaller source in the corner than standard iCSD to obtain the same potential. Summarizing, we expect the B methods to limit the magnitudes of the spurious sources at the boundary. In case of D methods this attenuation should be even stronger. We test both B and D variants because it is hard to tell a priori which boundary treatment leads to better reconstructions.

Jittering

The iCSD method allows us to calculate N unknown parameters of CSD distribution from N measuredpotentials. So far we assumed that the N unknowns were the values of CSD at the nodes placed next to the electrode positions, however, such an assumption is not the only possible. In fact, it leads to some constraints on the calculated CSD. For example, in the linear method the maxima and minima of the obtained current source density are always located at the nodes. One way to avoid this particular limitation is to use a different distribution, such as cubic spline approximation. Another way is to use an approach which we call "spatial jittering". In this variant we assume that the grid spanning CSD is slightly displaced with respect to the distribution of the electrodes (maximally by half of the cube size in each direction), see Fig. 3. The CSD obtained in this way is a valid solution of the inverse problem, that is, it also produces the measured potentials. We can now randomly choose many displaced grids, calculate the CSD and then take the average. This method produces "smoother" CSD distributions, especially for step and linear methods. Due to the linearity of this procedure the average obtained by jittering also generates experimentally obtained potentials and is an equivalent solution of the inverse problem.

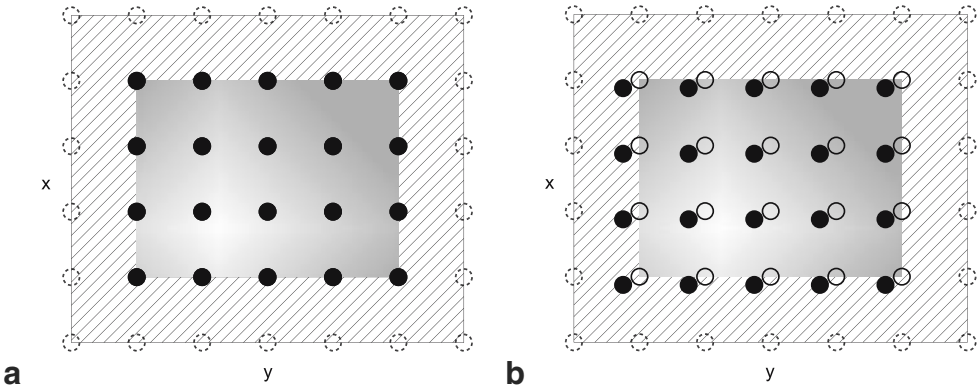

Fig. 3 The idea of spatial jittering. **a** The CSD distribution as in B or D method. **b** Jittering, grid spanning the sources (*empty circles*) is displaced with respect to the array of electrodes (*the black dots*)

The jittering is implemented by altering the F matrix. Let $\vec{d} = (d_x, d_y, d_z)$ be a displacement vector, that means the CSD grid is shifted by $\vec{d}$ with respect to potentials (electrode) grid. Then the elements of F (in case of "step" distribution) are given by the formula:

$$F_{ij} = \frac{1}{4\pi\sigma} \int_{x_j-\frac{1}{2}}^{x_j+\frac{1}{2}} \int_{y_j-\frac{1}{2}}^{y_j+\frac{1}{2}} \int_{z_j-\frac{1}{2}}^{z_j+\frac{1}{2}} \frac{\mathrm{d}z\,\mathrm{d}y\,\mathrm{d}x}{\sqrt{(x_i - d_x - x)^2 + (y_i - d_y - y)^2 + (z_i - d_z - z)^2}} \,.$$

We always use jittering in combination with either B or D boundary conditions, which we denote by J and K respectively. The number of displacement vectors used in the tests varied from 12 to 46. The vectors were chosen from a uniform distribution over the box of edge length 1 (equal to the distance between the grid points) centered at 0, aligned along the grid axes.

Results

Reconstruction Fidelity for Test Data

To compare quantitatively the different variants of iCSD method in three dimensions we used the reconstruction error defined as follows. We take an artificial current-source distribution C and calculate the potentials which would be measured by the three-dimensional array of electrodes. Then we use the potentials at the nodes to reconstruct CSD. The total reconstruction error is then the total square difference between the original, C, and the reconstructed, C_{rec}, densities, normalized as follows:

$$e = \frac{\int_1^{n_x}\int_1^{n_y}\int_1^{n_z} (C - C_{\mathrm{rec}})^2\,\mathrm{d}z\,\mathrm{d}y\,\mathrm{d}x}{\int_1^{n_x}\int_1^{n_y}\int_1^{n_z} C^2\mathrm{d}z\,\mathrm{d}y\,\mathrm{d}x} \,. \tag{6}$$

Other measures of reconstruction error we used are: squared maximal error ($\max |C - C_{\mathrm{rec}}|^2$), normalized with $\langle C^2 \rangle$ (mean of C^2), and 0.95/0.99-errors. We define the p-error as the smallest value δ such that the probability to find $\frac{|C-C_{\mathrm{rec}}|^2}{\langle C^2 \rangle} < \delta$ is p. This is easy to find from the cumulative distribution function of square errors $cdf(\frac{|C-C_{\mathrm{rec}}|^2}{\langle C^2 \rangle})$. On the graph of cdf one draws a horizontal line at $y = p$ and reads off the x axis the value of δ (see Fig. 4b). These measures help to differentiate between the reconstructions of comparable mean square error but with different smoothness properties.

The different measures of reconstruction error are presented in Tables 1 to 4. Each table collects the results for various reconstruction methods applied to given sets of test data.[6]

We compared all the iCSD methods presented in the previous section, that means all combinations of the assumed distributions (step, linear, natural spline, not-a-knot spline) and the boundary conditions (standard, B, D, jittering J, jittering K). The direct comparison with the "traditional" CSD is not possible because then we do not have the reconstructed CSD at the boundary nodes. In order to have a "traditional" method for comparison we generalize the Vaknin procedure to three dimensions, although it does not seem well justified. We extend the potentials grid by adding one point in each direction and duplicating the potential values, then we calculate the approximate Laplacian, Eq. 4. Hence we obtain the CSD values at all the grid points. To compare such reconstructed CSD to the actual sources we

[6]Even though the reconstruction errors are normalized with respect to the original sources we think that one should still be careful when comparing the results between different sets.

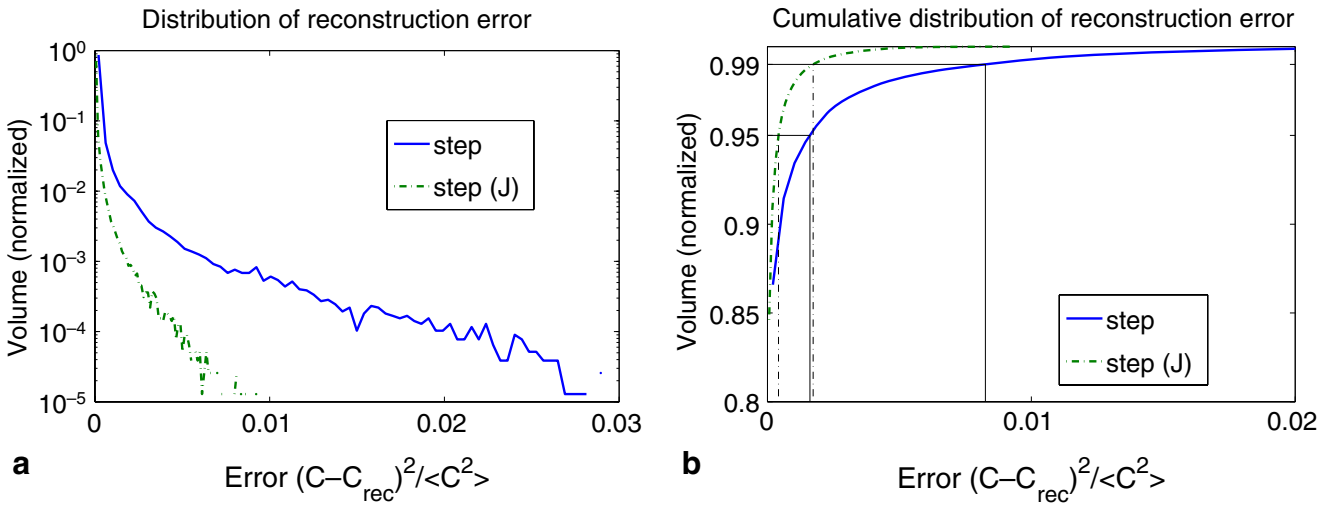

Fig. 4 Example of distribution (**a**) and cumulative distribution (**b**) of the reconstruction error for step and step J iCSD methods. *Vertical lines* define 0.95/0.99 errors. Unit normalized volume corresponds to the volume spanned by the electrodes grid. Here the step (J) method used 17 jittering vectors drawn from uniform distribution over $[-0.5, 0.5]^3$ cube

interpolate it between the grid points using splines. We denote this approach on figures and in tables by "trad (V) int".

It appears from our analysis that the relative utility of the methods depends on the type of the chosen test data. This is not surprising: if the test distribution was of the same type as the one assumed in the given iCSD variant then this (and only this) method would reconstruct the test data *exactly*. Therefore, an important question is what test data are "natural", that means resembling the CSD in actual tissue. We used five types of test data. The first four types were Gaussian sources with CSD given by the formula

$$C(\vec{r}) = A \exp\left(-\frac{(\vec{r}-\vec{r}_0)^2}{l}\right) .$$

There were between 4 and 8 such sources and the parameters A, l, $\vec{r}_0$ were chosen randomly. In the first type of data we assumed that CSD outside the electrode array was strictly zero and we truncated the distribution accordingly. In the second type we assumed that the CSD is non-zero in one additional layer of unit thickness, in the third type there were two additional layers. The fourth type was similar to the second but there was an additional strong point-like source located outside the grid. The fifth type of the test data were homogeneous spherical sources with sharp cut-off. For the tests we assumed the same configuration of electrode locations as in the motivating experiment which was a grid of size $4 \times 5 \times 7$.

First we compared the reconstruction fidelity of four different forms of assumed distributions (see Fig. 5 and Table 1). The test data were of the first type, that is the sources were truncated outside the grid. The results are as expected: the step method is the worst, the linear approximation of the distribution is an order of magnitude better, the natural splines are even better. The not-a-knot splines do not work very well on such data, they are worse than natural splines and even slightly worse than linear approximation (data not shown). The traditional method performs here rather poorly.

Note that the data presented in rows 2 and 3 should be interpreted differently than the other rows. These data are plotted with filled circles to emphasize the fact that we only know the values at the grid points. The figures for step method (row 5), on the other hand, are shown as squares because that is the assumed form of the CSD distribution reconstructed with this method. However, one could do a similar formal trick as we did with the "trad V" method, that is assume the calculated value at the grid point for the "step" distribution and spline-approximate the CSD between the grid points.

Table 1 The reconstruction errors for test data shown in Fig. 5

Method	Reconstruction error			
	Total	Max	0.95	0.99
Trad V int	0.16	8.5e−3	7.4e−4	2.8e−3
iCSD step	0.31	7.4e−3	1.4e−3	2.9e−3
iCSD step int	0.070	4.2e−3	2.5e−4	9.8e−4
iCSD linear	0.013	1.5e−3	6.9e−5	1.7e−4
iCSD spline (natural)	4.8e−3	2.5e−4	2.2e−5	4.8e−5

Table 2 The reconstruction errors for test data shown in Fig. 6

Method	Reconstruction error			
	Total	Max	0.95	0.99
Trad V int	0.32	0.048	9.6e−4	7.4e−3
iCSD spline	11	26	0.17	0.17
iCSD spline B	0.24	0.028	9.3e−4	5.0e−3
iCSD spline D	0.25	0.034	6.8e−4	5.2e−3
iCSD spline J	0.24	0.028	9.3e−4	4.6e−3
iCSD spline K	0.24	0.034	6.8e−4	4.8e−3

This is shown in row 6. Note, however, that proceeding in this way is inconsistent with the assumption of the uniform distribution in the boxes centered on the grid points. To obtain smooth CSD estimates one should rather assume some other kind of CSD distribution a priori. The smoothed step performs here better than "trad V int", but still much worse than linear. We expect that in all the remaining tests the performance of the "iCSD step int" method would be somewhere between the "trad V int" and the more sophisticated iCSD methods such as splines. The only advantage of using the "iCSD step int" would be that it is the easiest of the iCSD methods to implement. However, the gain in terms of computation time is minimal. The calculation of the F matrix is substantially faster than, for example, in spline method; however, the F matrix may be calculated once and then used for the whole analysis. Therefore we do not consider the "iCSD step int" method in the subsequent analysis and suggest the use of the spline iCSD.

Next we tested different boundary conditions (see Fig. 6 and Table 2, the splines used here are "not-a-knot"). As the boundary conditions are devised to deal with sources outside the grid, the test data here are of the second type (non-zero CSD assumed also in the additional layer). For such test data the "standard" iCSD method produces spurious sources at the boundary and the reconstruction error is very high. The quality of the method improves substantially if we use any of the variants pushing the boundary away. We also considered other forms of distributions but in the case at hand the appropriate treatment of the boundary seems much more important than the choice of the interpolation method. The traditional method is quite good here, with the error only about thirty percent larger than the iCSD.

The distortions present in the iCSD spline (second row in Fig. 6) form a characteristic pattern. We observed very similar patterns in experimental rat data (when processed without taking into account the boundary effects) and it seems to us that they can be classified as artifacts resulting from the sources located outside the grid. In the experimental situation these can be, for example, sources in the neighboring cortex.

It is even more important to choose suitable boundary treatment if we add a strong source to our data (the fourth type), see Fig. 7 and Table 3. For such data the methods ignoring the boundary are simply useless (cf. the second row in Fig. 7). The best method here is the traditional V method, but the iCSD not-a-knot spline K also performs well, although distortions are visible at the edges of the grid.

Our experience shows that the iCSD method (with appropriate boundary conditions) is usually better and never *much* worse than "trad V". The inverse methods seem to work comparably to "trad V" in case of compact sources, such as shown in Figs. 6 and 7, but are usually an order of magnitude better if we allow the sources to be larger, of the size observed in our experimental data, see Table 4 for two examples. The Vaknin

Table 3 The reconstruction errors for test data shown in Fig. 7

Method	Reconstruction error			
	Total	Max	0.95	0.99
Trad V int	1.3	0.045	4.5e−3	9.4e−3
iCSD spline	5.3e2	1.9e2	1.3	12
iCSD spline B	4.3	0.16	0.016	0.049
iCSD spline D	2.2	0.057	8.0e−3	0.018
iCSD spline J tone	4.1	0.16	0.016	0.045
iCSD spline K	2.2	0.056	7.8e−3	0.017

Table 4 The reconstruction errors for two sets of test data with large Gaussian sources

Method	Error for data set 1				Error for data set 2			
	Total	Max	0.95	0.99	Total	Max	0.95	0.99
Trad V int	0.34	0.014	2.0e−3	7.0e−3	0.14	2.1e−3	5.2e−4	1.0e−3
iCSD	2.5e−6	6.5e−4	3.0e−5	1.2e−4	5.1e−3	9.6e−5	2.5e−5	5.9e−5

Set 1: 4 sources, CSD non-zero only inside the grid. Set 2: 5 sources, CSD non-zero inside the grid with an additional layer added. The iCSD is a spline method taken with appropriate boundary conditions (standard for data set 1, B for data set 2)

procedure in one dimension is reported (Pettersen et al. 2006) to work better in case of balanced CSD, that means when the integral of the CSD over the region at hand is zero. Our study confirms this observation. If we first calculate the errors for a balanced current-source distribution and then change the sign of the sources so that they are all of the same sign then the errors in iCSD method grow twice while in "trad V" the errors grow four times. It is worth noting that for the data mentioned here the traditional method was two orders of magnitude worse, see Fig. 8. Another strong argument in favor of the inverse method is that here we make all our assumptions explicit: we must spell out the form of the current sources distribution. For the "trad

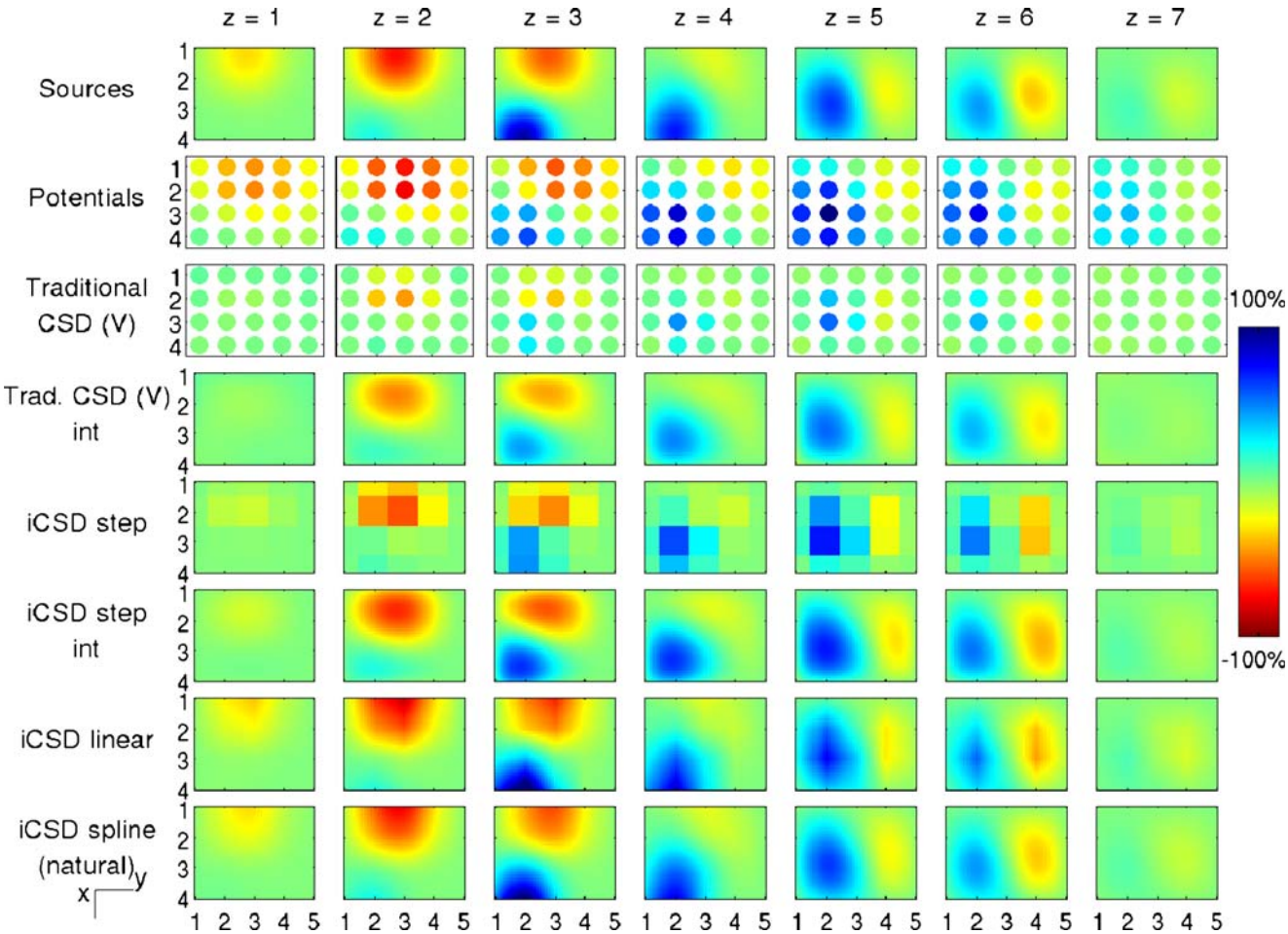

Fig. 5 Reconstruction of CSD from potentials (arbitrary units). *Each row* is a plot of a three-dimensional volume. From test sources (*the first row*) potential at the nodes is calculated (*second row*) and then passed on to various CSD methods. The traditional CSD (*third row*) gives the values of the CSD at grid points only. These are interpolated with splines to obtain the smoothed distribution (*fourth row*), the same method is used to smooth iCSD step. Test data were random Gaussian sources of comparable strength and different signs truncated at the boundary of the grid, see text for details. The values of the reconstruction errors are presented in Table 1

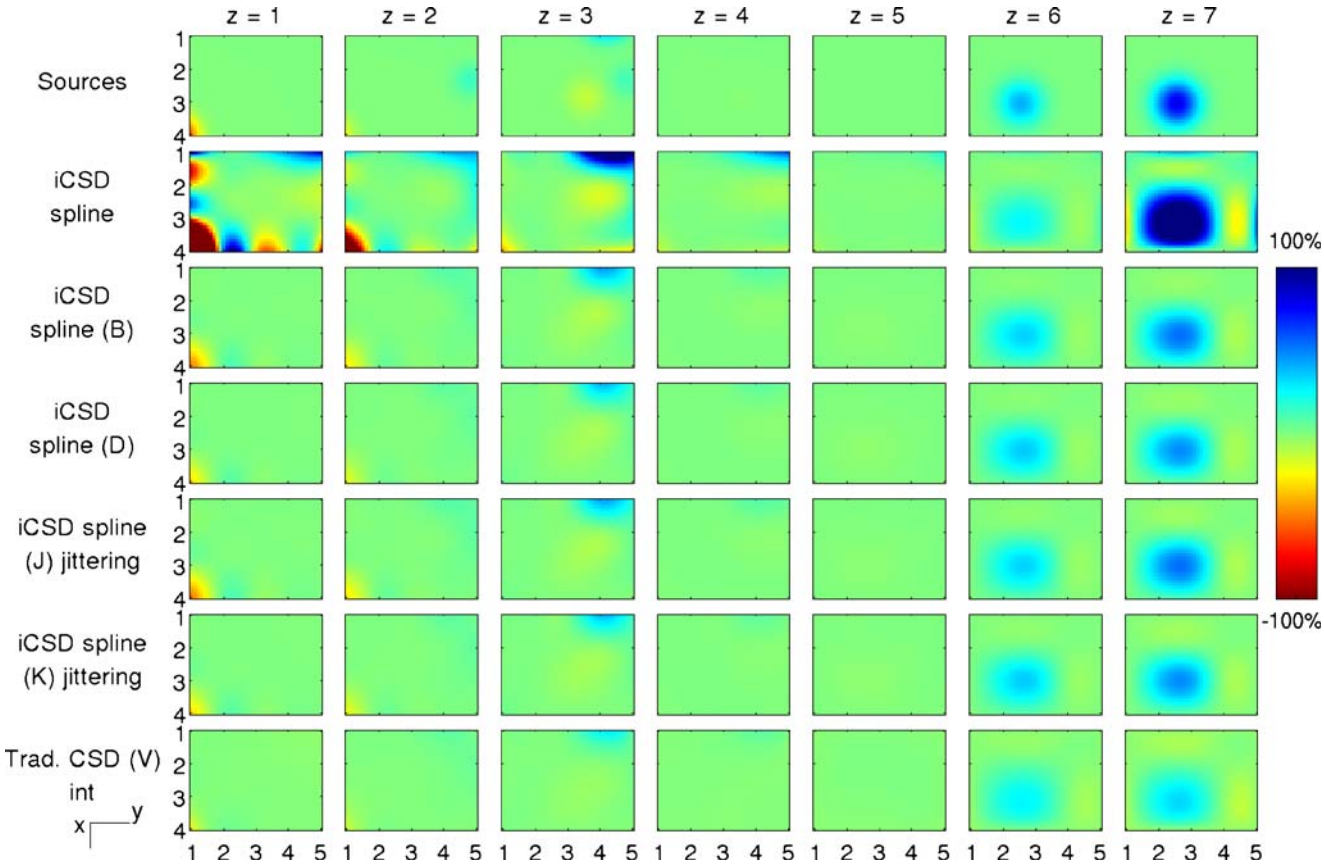

Fig. 6 Reconstruction of CSD from potentials, comparison of different treatments of the boundary (arbitrary units). Test data were random Gaussian sources truncated at the boundary of the grid extended by one layer in each direction, see text for details. Table 2 contains the values of reconstruction errors for this test

V" method we also make an assumption: potentials are constant outside the grid, but we do not know how that assumption is reflected in the reconstructed CSD. In our opinion it is much more elegant to make assumptions about the distribution of current-sources instead of the potentials.

The influence of jittering seems to differ strongly for various forms of assumed CSD distributions. In case of step (see Fig. 4) and linear distributions the jittering significantly improves the quality of the reconstruction, but for splines the improvement is only slight. It can be easily understood: the "step" reconstruction strongly depends on the choice of the sources grid, while the "spline" reconstruction does not.

Application to Evoked Potentials in Rat

The method was applied to LFPs recorded from deep structures of the rat forebrain. An adult male Wistar rat was anesthetized with urethane, placed in a stereotaxic apparatus, and a bunch of his left whiskers was glued to a piezoelectric stimulator. Most of the right parietal bone was removed and the resulting opening was covered with agar. A set of five stainless steel micro-electrodes (FHC, Bowdoin, USA; impedance of 1.5 MΩ at 1 kHz) mounted parallely in a sagittal plane (tips in antero-posterior line, spaced by 0.7 mm; the most anterior electrode 1.9 mm posterior to Bregma and 2.1 mm to the right from the midline) was lowered vertically through the opening and stopped each 0.7 mm at seven depths in the brain tissue, starting at 3.4 mm from the cortical surface. At each stop the bunch of left whiskers was deflected 60 times. LFPs were recorded monopolarly and allowed for extraction of 60 somatosensory evoked potentials (EPs) per each recording point. The length of the interelectrode distance was based on the average size of the studied thalamic nuclei (e.g. POm $1.4 \times 1 \times 2$ mm), and the expected large-scale activation evoked by the strong multi-whisker input.

The procedure was repeated at lateral positions 2.8, 3.5 and 4.2 mm to the right from midline, at

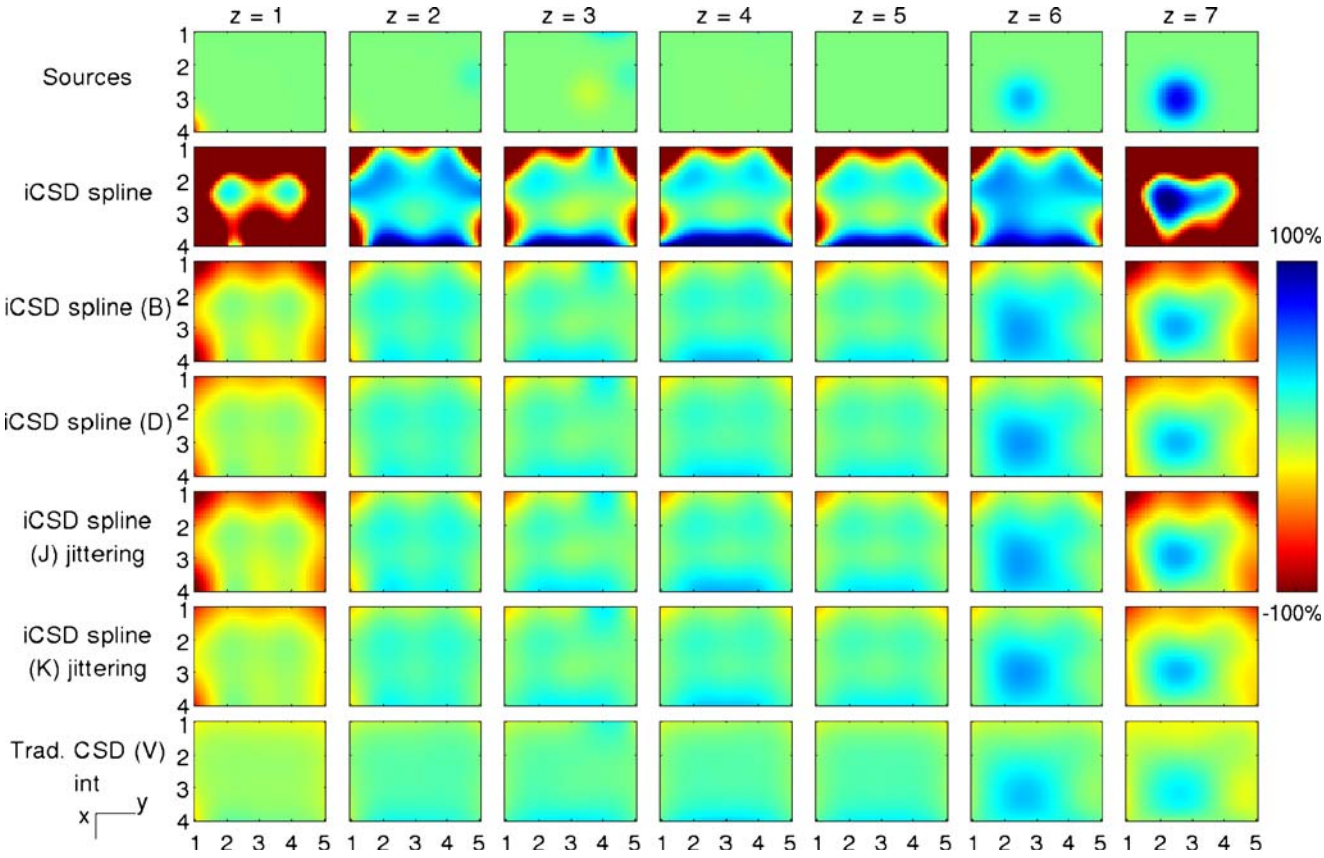

Fig. 7 Reconstruction of CSD from potentials. Test data were random Gaussian sources truncated at the boundary of the grid extended by one layer in each direction, plus an additional strong point source outside the grid was added at ($x = 6$, $y = 3$, $z = 4$), see text for details. Table 3 contains the values of reconstruction errors for this test

corresponding depths. Thus a rectangular grid of 140 ($4 \times 5 \times 7$) recording points comprising a slab of forebrain tissue with portions of the thalamus, pretectum, the hippocampus, and cerebral white matter was obtained. An exact location of the recording points was verified histologically after the experiment and anatomical structures were identified according to Paxinos and Watson (1996). For details of surgical procedure, stimulation of the vibrissae, signal processing and post-experimental procedure see Kublik et al. (2003).

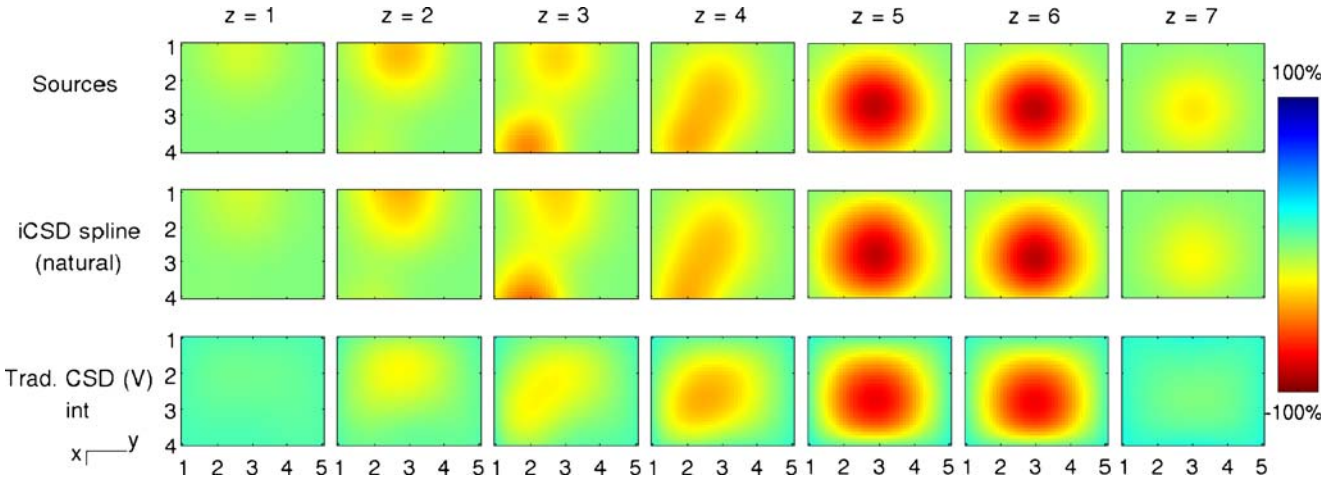

Fig. 8 Reconstruction of CSD from potentials for large and non-balanced current-sources located inside the grid (arbitrary units). The inverse method gives the total reconstruction error two orders of magnitude smaller than the traditional method. Note particularly the difference between the reconstructions at $z = 3$

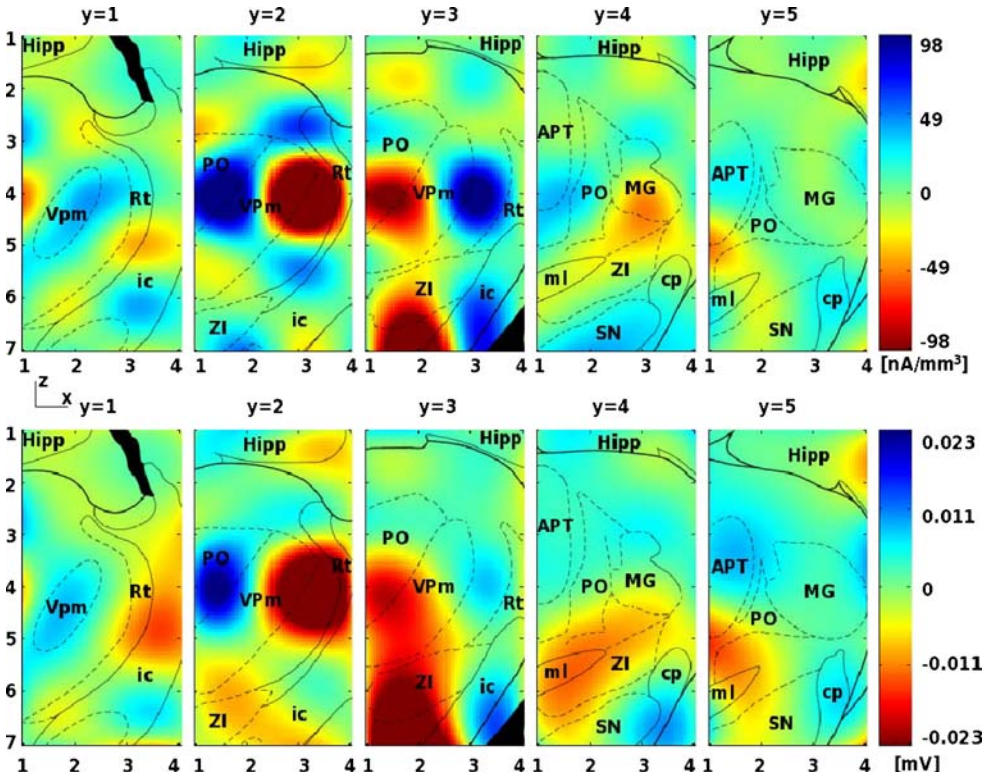

Fig. 9 *Top row*: Current source density 3.5 ms after the stimulus reconstructed using the iCSD not-a-knot spline D method. Note that different plane is shown than in the previous figures to allow usage of coronal brain sections. *Bottom row*: spline approximated potential in the tissue based on the same data as used for the CSD reconstruction at the same time. The grid spacing is 0.7 mm in each direction. For abbreviations see "Appendices"

The LFP signal was amplified (1,000 times) and filtered (0.1–5 kHz). Epochs (of about 1.4 s) containing EPs were digitized on-line (10 kHz) with 1401plus interface and Spike-2 software (CED, Cambridge, England). All stored data were examined for integrity and epochs with artifacts were excluded from further

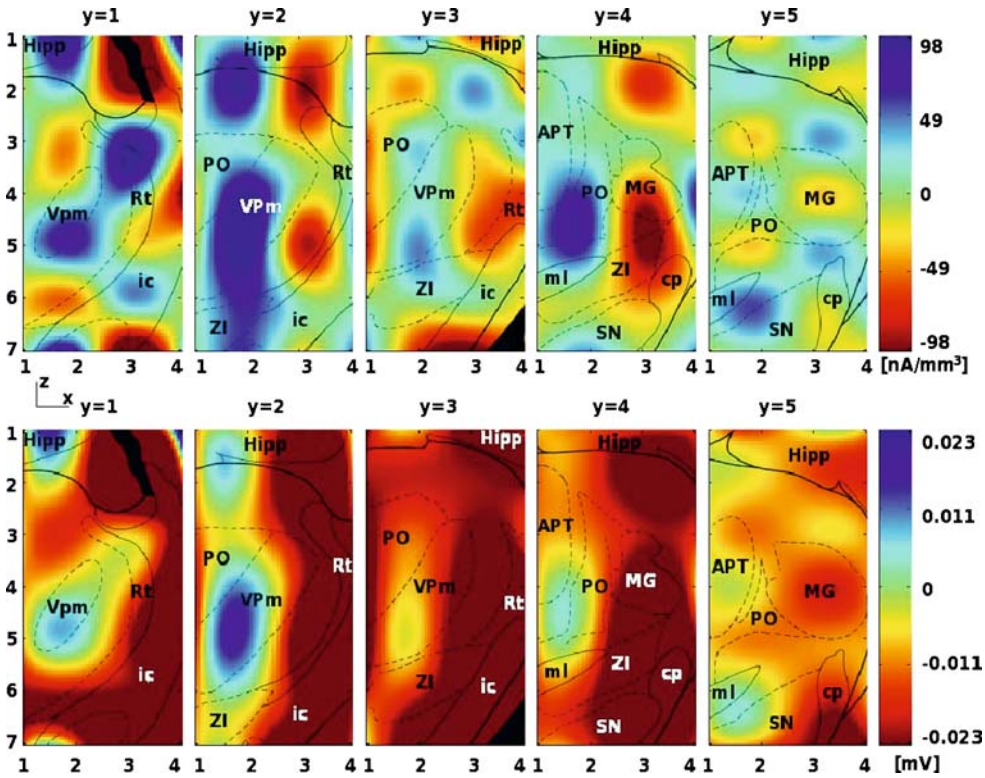

Fig. 10 As in Fig. 9, 15 ms after the stimulus

analysis. Recordings were stimulus averaged and smoothed with Savitsky–Golay filter of order 3 with window size 9 prior to further analysis.

Constant and isotropic conductivity of the tissue was assumed. We took $\sigma = 300\,\mathrm{S}\cdot\mathrm{mm}^{-1}$ as in (Hämäläinen et al. 1993; Nunez and Srinivasan 2005), although some measurements in the rat brain suggest that σ can take values around 60–70 $\mathrm{S}\cdot\mathrm{mm}^{-1}$ (Ueno and Sekino 2005). The only effect of accepting different values of σ would be a change of scale of reconstructed CSD.

Figure 9 shows the current source density 3.5 ms after the stimulus, reconstructed using the iCSD not-a-knot spline D method (top row). This is compared with a spline interpolation of the potentials used for the reconstruction (bottom row). There is a noticeable correlation, e.g. the activation blots around ($x = 1.5$, $z = 4$) and ($x = 3.5$, $z = 4$) at $y = 2$ slice in potentials have corresponding blots in CSD. However, the structure is clearly different, for instance a strong source visible in CSD around ($x = 3.5$, $y = 3$, $z = 4$) is almost invisible on the figure showing potentials.

The differences are even more dramatic at Fig. 10, which compares reconstructed CSD (top row) with spline approximation of potential in the tissue (bottom row) 15 ms after the stimulus. Here, the potential distribution seems to indicate strong activation of the whole region. The picture of CSD, while complicated, shows a clear structure of sources and sinks which one can attempt to understand by connecting the activation pattern with known anatomy of the somatosensory system.

The quality of comparison depends on the chosen scales in both kinds of figures (CSD, potentials). Our experience shows that one cannot choose a scale for potentials so that all the pictures have comparable intensities, which is possible for the CSD distribution in our case. This is another point in favor of studying the reconstructed CSD.

Discussion and Summary

LFPs measured in tissue are generated by macroscopic current flow resulting from concerted dynamics of neural populations. Long range nature of electric forces implies that every source can be visible in recordings at many sites complicating the analysis of electrophysiological data. Having the information about the distribution of the sources can dramatically improve the spatial resolution since these are often well localized in particular brain structures. Unfortunately, the problem of CSD reconstruction from finite number of recordings is ill-posed meaning that there are many different CSD distributions which could generate recorded potentials. There are also other problems which make reconstruction of CSD difficult. One of them is the lack of precise measurements of the electric conductivity tensor in the tissue. Another issue is that experimental measurements of potentials depend on the size of the electrode tip, as the recordings are local space averages of potential (see chapter 4 of Nunez and Srinivasan 2005). In our case, the electrode tip is so small in comparison with the interelectrode distance that the assumption of point-size seems to be justified. In cases where the effects of non-zero electrode size are significant one could include the effects of spatial averaging of the potentials in the construction of the matrix F. Despite these problems we believe that with a reasonable set of recordings at different sites the CSD reconstruction may provide the basic understanding of dynamics of an activation wave flowing through the investigated structure.

This leads to a question about which reconstruction method is optimal. Our experiments show that if we want to choose the best method for the problem at hand, it would be best to test the methods on sample CSD distribution, preferably from a realistic neural model. If that is not possible, then for well-localized sources we would recommend the inverse CSD method with natural spline distribution. If the sources are expected to be large and not confined to the probed volume then the recommended method would be not-a-knot splines with extended boundary. If the sources may be very small (localized) and/or the data are distorted by the presence of a strong source outside the grid, then the "traditional V" method may be useful, although the spline iCSD with boundary conditions should not be much worse.

The methods discussed in the present work constitute a framework which can be easily extended by considering other forms of CSD distributions, which may be case dependent, for instance anatomically motivated in specific cases. It is also a simple matter to develop similar formulae for two-dimensional case which will be of interest for electrode arrays recordings.

Information Sharing Statement

On page http://www.neuroinf.pl/Members/szleski/icsd.html we provide a set of MATLAB scripts used for the analysis of data implementing all the methods discussed in the text. These are provided as is without any warranty under GNU General Public License version 2.0 or later, in particular it may be freely changed and redistributed as long as the original authors are acknowledged.

One full set of data for a single rat is provided to allow for the generation of the movies which can also be found on the above webpage. The data can be used for research purposes, in particular for testing other methods of data analysis as long as this article is acknowledged in a published account of the results.

Acknowledgements We are grateful to Wit Jakuczun for his suggestion to investigate spatial jittering as one way to improve the CSD reconstruction. This work was partly financed from the Polish Ministry of Science and Higher Education research grants N401 146 31/3239 and 2P04C 046 27.

Appendices

Linear iCSD Method

In this appendix we construct the F matrix for the linear distribution of CSD. Consider a grid of points (i, j, k), where $i = 1..n_x$, $j = 1..n_y$, $k = 1..n_z$. Let us number the points with a multi-index $\alpha \equiv (i, j, k)$ and write $(i, j, k) \equiv (x_\alpha, y_\alpha, z_\alpha)$. Let V be the set of 8 vectors (v_1, v_2, v_3), $v_i \in \{0, 1\}$. The grid has $n = n_x n_y n_z$ nodes and there are $m = (n_x - 1)(n_y - 1)(n_z - 1)$ boxes spanned by these nodes. We index the boxes so that the corners of the box number α are $\alpha + v$ for $v \in V$. Let B denote the set of all the allowed indices α numbering the boxes and G stand for all the grid points. Let C denote the vector of CSD values at the nodes, that is $C_\alpha = C(x_\alpha, y_\alpha, z_\alpha)$ for $\alpha \in G$. We assume that CSD in boxes is given by a linear approximation.

Take a point (x, y, z) in box number α and let $\delta x = x - x_\alpha$, $\delta y = y - y_\alpha$, $\delta z = z - z_\alpha$. The value of CSD at this point obtained with the linear interpolation is given by:

$$C(x, y, z) = \sum_{v \in V} [1 - v_1 + (2v_1 - 1)\delta x] \times \left[1 - v_2 + (2v_2 - 1)\delta y\right] \times [1 - v_3 + (2v_3 - 1)\delta z]\, C_{\alpha+v}.$$

Therefore the distribution inside the box is a linear combination of 8 functions f_l, $l = 1..8$: $f_1 = 1$, $f_2 = \delta x$, $f_3 = \delta y$, $f_4 = \delta z$, $f_5 = \delta x \delta y$, $f_6 = \delta x \delta z$, $f_7 = \delta y \delta z$, $f_8 = \delta x \delta y \delta z$, with coefficients depending linearly on the values of C at the nodes of the box:

$$C(x, y, z) = \sum_{\beta \in G} \sum_{l=1}^{8} E^l_{\alpha\beta} f_l C_\beta.$$

The coefficients $E^l_{\alpha\beta}$ are non-zero only for $\beta - \alpha \in V$ and follow from the above formula, e.g. $E^1_{\alpha,\beta} = 1$ for $\beta - \alpha = (0, 0, 0)$, otherwise $E^1_{\alpha,\beta} = 0$, etc. The potential generated by such a distribution of current-source density at some point $(\tilde{x}, \tilde{y}, \tilde{z})$ is

$$\Phi(\tilde{x}, \tilde{y}, \tilde{z}) = \sum_{\alpha \in B} \sum_{\beta \in G} \sum_{l=1}^{8} F^l_\alpha(\tilde{x}, \tilde{y}, \tilde{z})\, E^l_{\alpha\beta} C_\beta \ ,$$

where

$$F^l_\alpha(\tilde{x}, \tilde{y}, \tilde{z}) = \frac{1}{4\pi\sigma} \int_0^1 \int_0^1 \int_0^1 \frac{f_l(x, y, z)\ \mathrm{d}z\, \mathrm{d}y\, \mathrm{d}x}{\sqrt{(\tilde{x} - x_\alpha - x)^2 + (\tilde{y} - y_\alpha - y)^2 + (\tilde{z} - z_\alpha - z)^2}} \ .$$

If we now take as $(\tilde{x}, \tilde{y}, \tilde{z})$ one of the grid points γ then

$$\Phi_\gamma = \sum_{\beta \in G} F_{\gamma\beta} C_\beta,$$

where

$$F_{\gamma\beta} = \sum_{\alpha \in B} \sum_{l=1}^{8} F^l_\alpha(x_\gamma, y_\gamma, z_\gamma)\, E^l_{\alpha\beta}.$$

Thus $F_{\gamma\beta}$ represents the direct and indirect contributions to the total potential at point γ from the CSD associated with the grid point β.

Spline iCSD Method

The construction of the F matrix for the spline distribution is in principle very similar to the case of linear distribution, but the level of complication is much higher. Similarly as in the previous appendix we have n nodes and m boxes, but now the interpolating function in each box is the three-dimensional cubic spline. That means there are $4 \times 4 \times 4 = 64$ base functions. Therefore there will be 64 each of E^ℓ and F^ℓ matrices. The main challenge here is to construct the E^ℓ matrices, that means to describe how a CSD value associated with a given node influences the interpolating splines in all the boxes.

First we briefly remind the construction of one-dimensional spline (Press et al. 1992). Suppose we have values of a function f at points $x = 1..n_x$. For x such that $j \le x \le j + 1$ define $P_1(x) = j + 1 - x$, $P_2(x) = x - j$. The formula

$$f(x) = P_1(x) f(j) + P_2(x) f(j + 1) \qquad (7)$$

gives a linear approximation, that means an approximation with a continuous function. In case of cubic splines we want more: we want also the first and second derivatives to be continuous. This can be done if we replace the right hand side of Eq. 7 with a third-degree polynomial:

$$f(x) = P_1(x)\,f(j) + P_2(x)\,f(j+1) + P_3(x)\,f''(j) + P_4(x)\,f''(j+1)\ , \tag{8}$$

where $P_3(x) = \frac{1}{6}(P_1(x)^3 - P_1(x))$, $P_4(x) = \frac{1}{6}(P_2(x)^3 - P_2(x))$. This formula guarantees that both f and its second derivative are continuous. The values of the second derivative f'' of f at nodes are a priori unknown, but can be calculated from the condition that also the first derivative is continuous. This condition leads to the following system of equations ($j = 2..n_x - 1$):

$$\frac{1}{6}f''(j-1) + \frac{1}{3}f''(j) + \frac{1}{6}f''(j+1) = f(j+1) - 2f(j) + f(j-1)\ .$$

There are n unknown $f''(j)$ and only $n-2$ equations, therefore we need two additional conditions. There are several commonly used choices for these conditions. One of them is to add equations

$$f''(1) = 0\ , \qquad f''(n) = 0\ ,$$

which leads to so-called "natural splines". The splines implemented in Matlab use a different set of conditions, namely

$$f''(3) - f''(2) = f''(2) - f''(1)\ ,$$

$$f''(n) - f''(n-1) = f''(n-1) - f''(n-2)\ .$$

These conditions mean that the *third* derivative is continuous at $x = 2$ and $x = n-1$ and they lead to what is known as "not-a-knot" splines. The important thing is that in both cases the values of f'' at the nodes can be obtained from $f(j)$, $j = 1..n$, by a linear operation which we call G:

$$f''(i) = \sum_{j=1}^{n} G_{ij} f(j)\ .$$

The matrix G is different for "natural" and "not-a-knot" splines.

The three-dimensional spline interpolation is obtained simply by performing three one-dimensional splines. The complication is that we do not want the values of the interpolating function at some points, but the coefficients standing by the base functions. We found that it is convenient to choose base functions which are products of the polynomials P_1, P_2, P_3, P_4 of variables x, y and z, that means $P_1(x)P_1(y)P_1(z)$, $P_1(x)P_1(y)P_2(z)$, …, $P_4(x)P_4(y)P_4(z)$. To extract the coefficients we start with the spline in z direction:

$$f(x,y,z) = P_1(z)\,f(x,y,j) + P_2(z)\,f(x,y,j+1) + P_3(z)\,f_{zz}(x,y,j) + P_4(z)\,f_{zz}(x,y,j+1)\ , \tag{9}$$

where f_{zz} stands for $\frac{\partial^2 f}{\partial z^2}$ and is given by $f_{zz}(x,y,j) = \sum_{i=1}^{n_z} G^z_{ji} f(x,y,i)$. Therefore we reduce the problem to two-dimensional splines in the xy-plane. We continue with

$$f(x,y,j) = P_1(y)\,f(x,i,j) + P_2(y)\,f(x,i+1,j) + P_3(y)\,f_{yy}(x,i,j) + P_4(z)\,f_{yy}(x,i+1,j)\ , \tag{10}$$

and so on. In the end we get the coefficients standing by the base functions as combinations of $f(i,j,k)$ (values of f at the nodes) and the matrices G^x, G^y, G^z. Then we construct the matrices $E^{pqr}_{\alpha\beta}$, $\alpha \in B$, $\beta \in G$, $1 \le p,q,r \le 4$. The number $E^{pqr}_{\alpha\beta}$ is the coefficient standing by $P_p(x)P_q(y)P_r(z)$ in box α resulting from a unit CSD at the node β. The construction of 64 $F^{pqr}_{\gamma\alpha}$ matrices (each of size n by m), where $\gamma \in G$ and $\alpha \in B$, is simple:

$$F^{pqr}_{\gamma\alpha} = \frac{1}{4\pi\sigma}\int_0^1\int_0^1\int_0^1 \frac{P_p(x)P_q(y)P_r(z)}{\sqrt{(x_\gamma - x_\alpha - x)^2 + (y_\gamma - y_\alpha - y)^2 + (z_\gamma - z_\alpha - z)^2}}\mathrm{d}z\mathrm{d}y\mathrm{d}x\ ,$$

and the full matrix F is now

$$F = \sum_{p,q,r=1}^{4} F^{pqr} E^{pqr}\ ,$$

or

$$F_{\gamma\beta} = \sum_{p,q,r=1}^{4}\sum_{\alpha=1}^{m} F^{pqr}_{\gamma\alpha} E^{pqr}_{\alpha\beta}\ .$$

Anatomical Abbreviations

APT	anterior pretectal nucleus
cp	cerebral peduncle
Hipp	hippocampus
ic	internal capsule
MG	medial geniculate nucleus
ml	medial lemniscus
PO	posterior thalamic nuclear group
Rt	reticular thalamic nucleus
SN	substantia nigra
VPm	ventral posteromedial thalamic nucleus
ZI	zona incerta

References

Freeman, J. A., & Nicholson, C. (1975). Experimental optimization of current source-density technique for anuran cerebellum. *Journal of Neurophysiology, 38*, 369–382.

Hämäläinen, M., Hari, R., Ilmoniemi, R. J., Knuutila, J., & Lounasmaa, O. V. (1993). Magnetoencephalography—theory, instrumentation, and applications to noninvasive studies of the working human brain. *Reviews of Modern Physics, 65*, 413–497.

Kublik, E., Świejkowski, D. A., & Wróbel, A. (2003). Cortical contribution to sensory volleys recorded at thalamic nuclei of lemniscal and paralemniscal pathways. *Acta Neurobiologiae Experimentalis (Wars), 63*, 377–382.

Lin, B., Colgin, L. L., Brücher, F. A., Arai, A. C., & Lynch, G. (2002). Interactions between recording technique and AMPA receptor modulators. *Brain Research, 955*, 164–173.

Mitzdorf, U. (1985). Current source-density method and application in cat cerebral cortex: Investigation of evoked potentials and eeg phenomena. *Physiology Review, 65*, 37–100.

Nicholson, C., & Freeman, J. A. (1975). Theory of current source-density analysis and determination of conductivity tensor for anuran cerebellum. *Journal of Neurophysiology, 38*, 356–368.

Novak, J. L., & Wheeler, B. C. (1989). Two-dimensional current source density analysis of propagation delays for components of epileptiform bursts in rat hippocampal slices. *Brain Research, 497*, 223–230.

Nunez, P. L., & Srinivasan, R. (2005). *Electric fields of the brain: The neurophysics of EEG.* Oxford University Press.

Paxinos, G., & Watson, C. (1996). *The rat brain in stereotaxic coordinates, compact third edition* Academic.

Pettersen, K. H., Devor, A., Ulbert, I., Dale, A. M., & Einevoll, G. T. (2006). Current-source density estimation based on inversion of electrostatic forward solution: Effects of finite extent of neuronal activity and conductivity discontinuities. *Journal of Neuroscience Methods, 154*, 116–133.

Plonsey, R., (1969). *Bioelectric phenomena.* New York: McGraw-Hill Book Company.

Press, W. H., Teukolsky, S. A., Vetterling, W. T., & Flannery, B. P. (1992). *Numerical Recipes in C: The art of scientific computing*, chapter 3.3 (2nd ed.) (pp. 113–115). Cambridge University Press.

Shimono, K., Brucher, F., Granger, R., Lynch, G., & Taketani, M. (2000). Origins and distribution of cholinergically induced beta rhythms in hippocampal slices. *Journal of Neuroscience, 20*, 8462–8473.

Sukov, W., & Barth, D. S. (1998). Three-dimensional analysis of spontaneous and thalamically evoked gamma oscillations in auditory cortex. *Journal of Neurophysiology, 79*, 2875–2884.

Ueno, S., & Sekino, M. (2005). Conductivity tensor MR imaging. *Proceedings of the XXVIIIth URSI General Assembly in New Delhi*.

Vaknin, G., DiScenna, P. G., & Teyler, T. J. (1988). A method for calculating current source density (CSD) analysis without resorting to recording sites outside the sampling volume. *Journal of Neuroscience Methods, 24*, 131–135.